Indian Journal of Pure & Applied Physics
Vol. 55, November 2017, pp. 813-820

The growth of the silver nanoparticles on the mesoporous silicon and macroporous silicon: A comparative study

Alwan Mohammed Alwan[a], Ali Ahmed Yousif [b] & Layla Alag Wali[c]*

[a]Department of Applied Sciences, University of Technology , Baghdad, Iraq

[b]College of Education, Al – Mustansiriyah University, Baghdad, Iraq

[c]College of Basic Education, Al – Mustansiriyah University, Baghdad, Iraq

Received 13 November 2016; accepted 3 May 2017

Two porous silicon (PS) layers, namely mesoPS and macroPS have been prepared by electrochemical etching (ECE) and photo–electrochemical etching (PECE) processes, respectively. The surface morphology of mesoPS and macroPS reflects a different form of morphology. Silver nanoparticles (AgNPAs) have been obtained through immersion of PS samples in $AgNO_3$ solution. The mechanism of Ag growth depends on the substrate morphology. In the case of using mesoPS substrate, the AgNPAs have sizes ranging from 0.25 to 2.25 μm, so they can't enter inside pores and therefore they aggregate on the mesoPS surface, while by using macroPS substrate, they have sizes ranging from 0.1 to 1.5 μm, decorate the inner of the pores and the separate Ag nanoaggregates form on the macroPS surface. The highest SERS has been obtained for AgNPAs/macroPS substrate rather than AgNPAs/mesoPS substrate. The enhancement factor (EF) values achieved by using AgNPAs deposited on macroPS and mesoPS substrates are about (1.8×10^6) and (3.2×10^4), respectively.

Keywords: Porous silicon, Silver nanoparticles, Immersion plating, SERS

1 Introduction

Porous silicon (PS) has attracted much attention since the finding of its visible photoluminescence (PL) at room temperature[1]. Recently, it has been shown that PS can reduce positive metallicions since it acts as a modest reducing agent, therefore the nanoparticles of these metals can be spontaneously formed onto PS yielding surface enhanced Raman scattering (SERS)–active substrate[2-5].

PS can exhibit different morphologies and typical pore sizes, therefore it is characterized by its porosity (volumetric fraction of void within PS), its thickness, its internal surface (taking into account the pore surfaces), and its morphology (shape and pore size)[6]. The PS structures are categorized to the dominant pore diameter (d) as microPS ($d \leq 2$ nm), mesoPS (2 nm < d < 50 nm) and macroPS (d > 50 nm)[6,7].The resulting pore features of PS are strongly dependent on the doping type and orientation of the silicon (Si) substrate and the ECE factors[3,8-10].

The physicochemical properties of the AgNPAs, such as the surface plasmon resonance and big effective scattering cross section of individual AgNPAs make them perfect nominees for molecular labeling, where phenomena such as SERS can be subjugated[3,11,12], therefore the synthesis of Ag nanostructures has been an active research area because of their excellent optical properties, which strongly depend on size, shape and composition. A variety of methods has been used to synthesize the AgNPAs for instance, sonochemical synthesis, laser ablation, electrochemical way, thermal decomposition, and microwave irradiation[3,4,13,14]. However, practically all these methods are costly and require special technique. PS has a very large hydrogenated internal surface area[15,16], which plays an essential role in the deposition process of Ag on the PS layer by an efficient and simple method called an immersion plating[3,5]. Immersion of PS into silver nitrates ($AgNO_3$) solution performs an involuntary composition of AgNPAs by way of Ag ions reduction through Si–H bonds on the surface of the PS sample, as shown in the following equations[3]:

$$2Si_{(surf)} + H_2O \rightarrow Si - O - Si_{(surf)} + 2H^+_{(solution)} + 2e^-; \quad \ldots (1)$$

$$2Si - H_{(surf)} + H_2 \rightarrow Si - O - Si_{(surf)} + 4H^+_{(solution)} + 4e^-; \quad \ldots (2)$$

$$Ag^+_{(solution)} + e^- \rightarrow Ag_{(surf)} \quad \ldots (3)$$

*Corresponding author (E-mail: laylamncom@gmail.com)

The sensitivity of SERS strongly depends on the formation of electromagnetic "hotspots" sites, where the local electric field is very intense. Hence, at these sites, the Raman signals from molecules of the analyte are particularly strong and contribute to the main fraction of the overall Raman intensity[17].

In this work, the effects of the PS types (*p*–type mesoPS (mesoPS) and *n*–type macroPS (macroPS)) on the growth mechanism of the AgNPAs and corresponding SERS have been studied based on the analysis of the field emission scanning electron microscope (FE–SEM) images, X–ray diffraction pattern (XRD) and SERS.

2 Experimental Details

2.1 Chemical materials

Hydrofluoric acid (HF) of 48% concentration, ((CDH), India) was diluted with high purity ethanol (C_2H_5OH) of 99.9% concentration (Sigma-Aldrich, Germany) in order to prepare a required etching solution with a concentration of about 29% HF. $AgNO_3$ (Aldrich, 99.99%) was dissolved in triply distilled water for preparing a required $AgNO_3$ solution with a concentration of about (0.01 M) by using the following equation[18]:

$$\text{Molarity} = \frac{\frac{W}{M.Wt}}{V} \quad \text{.... (4)}$$

where, W (g) is the weight of the $AgNO_3$, $M.Wt$ (g/mole) is the molecular weight, and V (l) is the volume of the dissolved solution.

2.2 Preparation of PS samples

In this study, *p*–type (100) Si wafer and *n*–type (100) Si wafer with a resistivity of 10 Ω.cm were used as substrates for preparing mesoPS and macroPS, respectively. The dimensions of samples were 1.5×1.5 cm^2 exposed to the electrolyte which consisted of HF and absolute ethanol. The PS samples were prepared with a fixed etching current density of 14 mA/cm^2 and a fixed etching time of 25 min by ECE of *p*–type wafer and PECE of *n*–type wafer. A laser source with intensity of 30 mW/cm^2 and wavelength of 532 nm was used to illuminate *n*–type Si wafer. The etching process was performed at room temperature in a solution composed of a mixture (HF:C_2H_5OH=3:2). Si wafer acted as the anode electrode, while platinum (Pt) ring was used as the cathode electrode (Fig. 1). Prior to etching process, the samples were first cleaned in a mixture of (HF:C_2H_5OH=1:10) for 10 min to remove the native oxide layer on the surface of the Si and then washed with high purity ethanol.

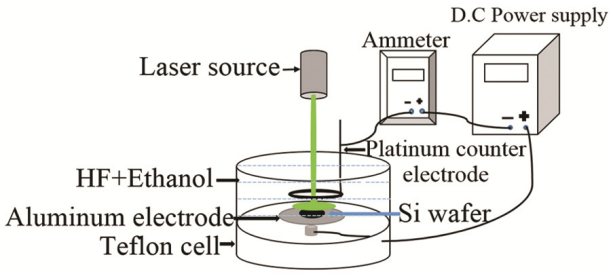

Fig. 1 — Schematic diagram of etching system with laser source and without laser source for PECE and ECE, respectively.

2.3 Fabrication of AgNPAs on PS layer

The AgNPAs were prepared at room temperature by immersion plating process. The fresh PS samples were immersed in the 0.01 M aqueous solution of $AgNO_3$ for 16 min to prepare sandwich structures of AgNPAs/mesoPS and AgNPAs/macroPS.

These structures were rinsed out in the HCl solution with a concentration of 0.01 M for 10 s in order to remove the contaminants adsorbed on the surfaces of AgNPAs/PS substrates, and then the AgNPAs/PS samples were incubated for 15 min in solution of R6G dye, which was used as analyte in this study. The specific weight of the dye was dissolved in ethanol to prepare the solutions of R6G dye with fixed concentration dye of 10^{-6} M by using Eq. (4), where the molecular weight of R6G dye is about 479.02 g/mol.

2.4 Characterizations

The crystal structure of mesoPS, macroPS, AgNPAs/mesoPS and AgNPAs/macroPS samples was tested by the experiments of XRD (XRD – 6000, Shemadzue). A power diffraction system with CuK_α X–ray tube (λ=0.154056 nm) was used. The morphology of same samples was examined by the FE–SEM (FE–SEM; MIRA3 TESCAN). The PL of the mesoPS and macroPS samples was examined by (PL; Cary Eclipse FL 0912M014) at room temperature using excitation laser wavelength of 325 nm. Raman spectra of R6G dye were measured with the dispersive Raman microscope (Almega Thermos Nicolet) using 532 nm of a Nd:YLF laser for excitation, the laser power was 30 mW. For each spectrum, the integration time was set as 2 s.

3 Results and Discussion

3.1 Morphological features of the fresh PS

The porosity, the porous layer thickness, and the surface topography which depend on the etching conditions are the most important morphological parameters of PS layer[15].

The porosity of mesoPS and macroPS was determined by a gravimetrical method using the following equation[19] :

$$P = \frac{m_1 - m_2}{m_1 - m_3} \quad \ldots (5)$$

where, m_1, m_2, m_3 are the Si wafer weight before the process of etching, after the process of etching and after removal of PS layer in a solution of NaOH, respectively. It is found that the porosity of the mesoPS and macroPS samples has been estimated as 54% and 77%, respectively. Figure 2(a,b,c) shows the surface morphology of mesoPS layer at different magnifications and the cross-sectional FE–SEM image of the sample. The structure of mesoPS is a pore look like, spherical and irregular in shape, and the pores are randomly distributed on the surface. The statistical distribution of the pore sizes shows that the pores are in the range of (3–39) nm, and the peak of the pore size distribution is about 9 nm, as shown in Fig. 2(d). The magnified image of Fig. 2(b) illustrates that the micrometer size pores are present on the surface, therefore big enough AgNPAs can form on the walls of the micropores, at the same time the pores aren't blocked by these nanoparticles and this leads to increase the effective surface of the sample[3]. As shown in the cross–sectional FE–SEM image of the mesoPS layer (Fig. 2(c)), the mesoPS layer thickness is about 77.58 µm, and this means that the vertical deep pores extend from the surface into the Si crystal.

Figure 3(a,b) depicts the FE–SEM images of the macroPS sample. From this image, it's clear that the porous structure has a pore–like structure with pore sizes ranging from 0.5 to 5.5 µm, and the peak of the pore size distribution is about 2.5 µm, as manifested in Fig. 3(d). The dark spots regions on the images are attributed to the pores formed, whereas the white area corresponds to the remaining Si. The images reveal that some pores are overlapping, and the pores are randomly distributed on the porous surface (Fig. 3(a,b)). As shown in the cross–sectional FE–SEM image of the porous layer (Fig. 3(c)), the macroPS layer thickness is about 2.8 µm, and it's easy to distinguish that the pore diameter changes gradually from the surface to the bulk.

This behavior is due to the fact that only the surface layers under illumination create the electron–hole pairs, therefore the etching rate will progressively reduce with the depth from the highest to the lowest layers yielding cone–like pores in PS structures[20]. This means that the nanocrystal at the PS/c–Si interface will become larger than the particles at the top of the nanostructure, so the layer seems as a double porous layer with a microPS on top of a macroPS, this behavior is confirmed by the PL spectrum, as shown in Fig. 4(b) later.

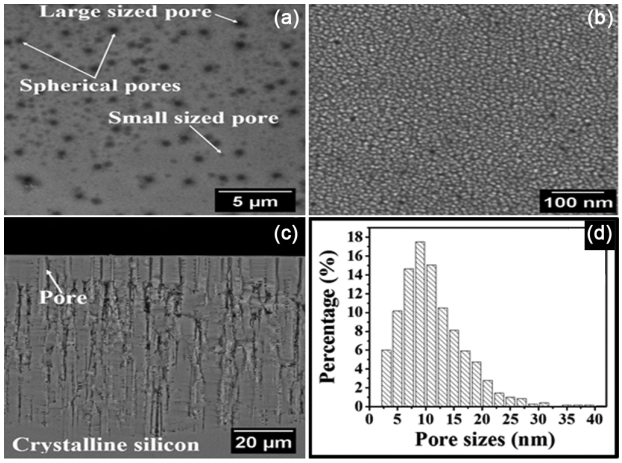

Fig. 2 — (a,b) FE–SEM images of mesoPS surface at scale bars of 5 µm and 100 nm, respectively, (c) cross–sectional FE–SEM image of mesoPS sample and (d) the statistical distribution of pore sizes for the sample.

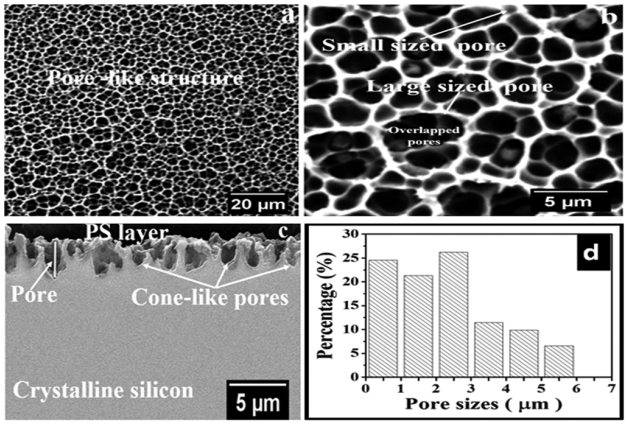

Fig. 3 — (a,b) FE–SEM images of macroPS surface at scale bars of 20 µm and 5 µm, respectively, (c) cross–sectional FE–SEM image of macroPS sample and (d) the statistical distribution of pore sizes for the sample.

3.2 PL properties of PS layer

PL spectra of PS are strongly dependent on the surface morphology of the porous layer[15]. Figure 4(a,b) shows the room temperature PL spectra of the mesoPS and macroPS samples, respectively. The PL spectrum of mesoPS sample depicts a single peak emission at 655.94 nm which corresponds to the energy gap of 1.89 eV, while the PL spectrum of macroPS has two peaks at 525.96 nm and 640.86 nm which correspond to the energy gaps of 2.36 eV and 1.94 eV, respectively. The appearance of the double peaks of PL is associated with the spatial size distribution of the nanocrystallites in macroPS sample as said before, the nanocrystal at the PS/c–Si interface is larger than the nanocrystal at the top of the PS structure, i.e., founding two PS layers on the porous structure. So, on exciting the macroPS structure, the peak at about 640.86 nm is due to the larger nanocrystals, and the peak at 525.96 nm is owing to the smaller nanocrystals. A small broadening and a large broadening of PL peak can be observed in Fig. 4(a,b), respectively. This is attributed to the distribution of nanosize particles since if it increases, the broadening of PL peak will increase and vice versa.

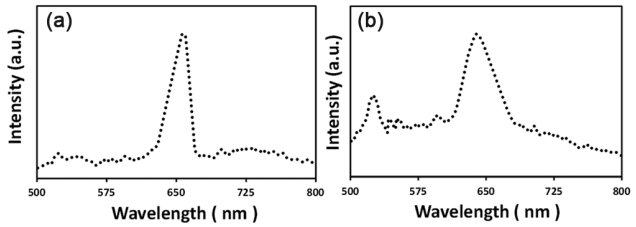

Fig. 4 — (a,b) PL spectra of mesoPS and macroPS

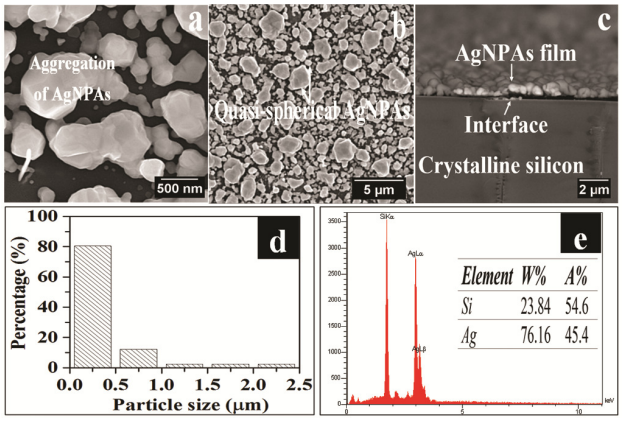

Fig. 5 — (a,b) FE–SEM images of AgNPAs/mesoPS surface with scale bars of 500 nm and 5 μm, respectively, (c) cross–sectional FE–SEM image, (d) the statistical distribution for the sizes of the AgNPAs deposited on mesoPS and (e) EDX analysis of the sample. The inserted table of Fig. 5(e) displays the percentage of each component on the sample surface.

3.3 Morphological properties of AgNPAs / PS

The immersion process of mesoPS and macroPS in $AgNO_3$ solution is an effective way to form the AgNPAs inside and outside the individual pores in the porous structure through the reduction process of Ag ions with the Si-H bonds[3]. The density, the size and the arrangement of the AgNPAs depend on the morphology of the underlying substrate[21]. For mesoPS, the surface morphology is illustrated in Fig. 5(a,b,c). From this figure, it's clear that the AgNPAs are located outside the pores in the porous structure. Because of the very small size of the pores in the mesoPS layer, the AgNPAs couldn't enter inside the pores; therefore they aggregated on the surface of the mesoPS. This means that the mesoPS morphology (spongiform) supplied a high density of suitable nucleation sites for the AgNPAs growth. This result is in a good agreement with that suggested by Giorgis *et al.*[2]. They have prepared AgNPAs with densely close–packed on the mesoPS surface. The statistical distribution for the resulting sizes of AgNPAs is presented in Fig. 5(d), and as shown from this figure, the Ag was deposited with the dispersion in size of particles ranging from 0.25 μm to 2.25 μm, and the peak of the AgNPAs is about 0.25μm.

For macroPS layer, the surface morphology is demonstrated in Fig. 6(a,b,c). From this figure, it's easy to distinguish that the AgNPAs are located inside the individual pores, and the AgNPAs growth follows the pore morphology since they are uniformly distributed on the surface.

Figure 6(c) shows that AgNPAs decorate the inner of the pores, and the pores are completely filled with AgNPAs. Furthermore, Fig. 6(b) views that the separated silver nanoaggregates are formed (islands of AgNPAs). This can be attributed to that the increase in the porosity leads to sharpen the surface roughness and so to increase the numbers of dangling Si bonds, which become passivated with hydrogen[16] (H), since the number of Si–H bonds plays a very important role in the process of Ag ions reduction[3]. The statistical distribution (Fig. 6(d)) for the sizes of AgNPAs reveals that the Ag is deposited with the dispersion in size of particles ranging from 0.1 μm to 1.5 μm, and the peak of the particle sizes is about 0.1 μm.

EDX was used to investigate the change in the surface composition of PS due to the coating by AgNPAs. Figure 5(e) displays the existence of Ag and Si elements on the AgNPAs/mesoPS sample, while Fig. 6(e) shows the existence of Si, Ag and oxygen

elements on the AgNPAs/macroPS sample. The existence of Si element is attributed to the Si substrate, and the existence of oxygen element on the AgNPAs/macroPS sample signifies the oxidation of Si.

3.4 XRD analysis

The XRD patterns of the mesoPS, macroPS, AgNPAs/mesoPS and AgNPAs/macroPS, respectively, are illustrated in Fig. 7(a,b,c,d) which shows that for all the PS samples one diffraction peak appeared at 2θ about of 33.26° which is assigned to the (100) plane of Si according to the standards (JCPDS). Figure 7(c,d) exhibits that two peaks appeared at 2θ about of 38.4° and 44.55° for the AgNPAs/mesoPS and at 2θ about of 38.28° and 44.47° for the AgNPAs/macroPS which are assigned to the (111)

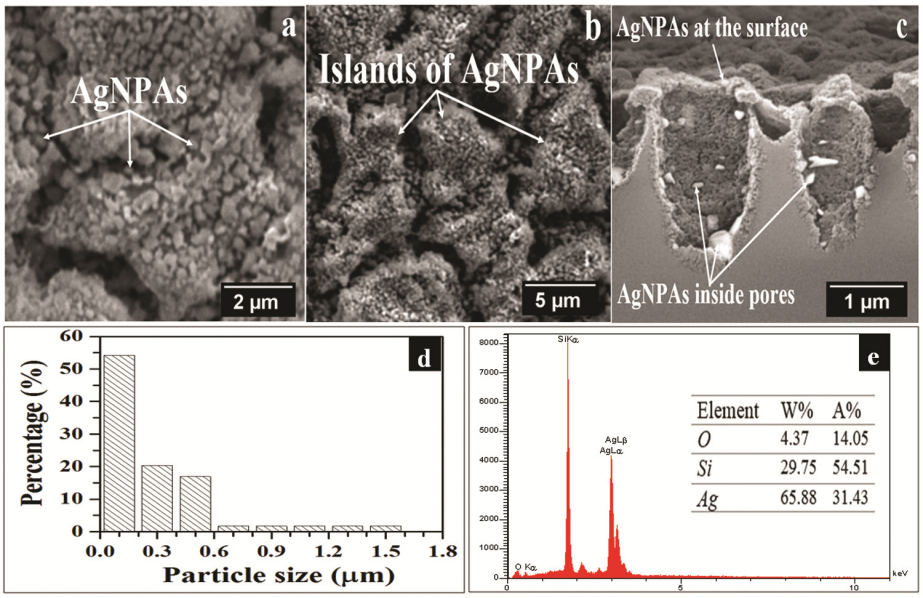

Fig. 6 — (a, b) FE–SEM images of AgNPAs/macroPS surface with scale bars of 2 µm and 5 µm, respectively, (c) cross–sectional FE–SEM image, (d) the distribution diagrams for the sizes of the AgNPAs deposited on macroPS and (e) EDX analysis of the sample. The inserted table in (e) displays the percentage of the each component on the sample surface.

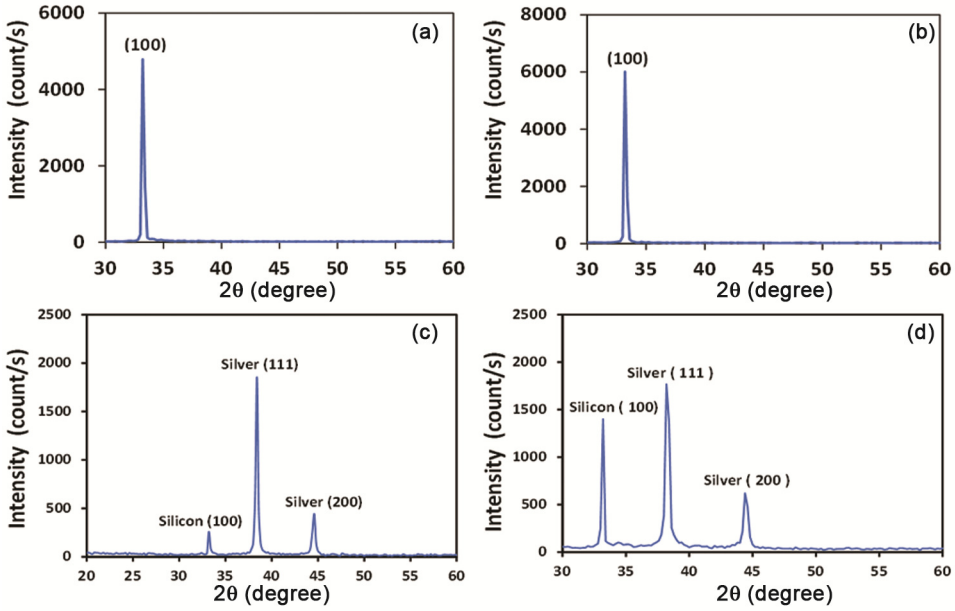

Fig. 7 — XRD patterns of the (a) mesoPS, (b) macroPS, (c) AgNPAs/mesoPS and (d) AgNPAs/macros.

and (200) crystal planes of Ag, respectively. They are compared with JCPDS, all the reflections match to pure Ag element with face centered cubic symmetry (FCC). This result is in agreement with the results reported in the literature[13,22]. The intensity of peaks demonstrated the great degree of the AgNPAs crystallinity. The diffraction of the peaks is obviously broadened as compared with bulk Ag, denoting the formation of AgNPAs. It is very clear that the Ag deposition process leads to the decreasing in the intensity of the reflection from the (100) plane of Si, this is attributed to the covering of the sample surfaces by the AgNPAs.

The structural parameters for AgNPAs are calculated from XRD results. The data are tabulated in the Table 1. The sizes of the AgNPAs (D_P) are calculated by using Scherrer's formula[23] as follows:

$$D_p = \frac{0.9\lambda}{\beta\cos\theta} \quad \ldots (6)$$

where, β is the full width at half maximum (radians), λ is the wavelength in nm of employed radiation, θ is the Bragg diffraction angle in degree and (0.9) is the shape factor value.

Specific surface area (S) is the property of the material. The AgNPAs have attracted much attention because they have a high specific surface area which can be calculated by using the following equation[24]:

$$S = \frac{6000}{D_p\rho} \quad \ldots (7)$$

where, ρ is the density of Ag 10.5 g/cm^3, since it is found for (111) direction that the size and specific surface area of AgNPAs are 17.26 nm and 33.41 m^2/g, respectively, for sample Ag/mesoPS and 16.3 nm and 35.09 m^2/g for sample AgNPA/macroPS, respectively.

Since the FE–SEM images indicate the aggregated particle sizes, the grain sizes of the AgNPAs/mesoPS and AgNPAs/macroPS samples which were determined from the XRD data are smaller than that obtained from the FE–SEM images. The bigger nanoparticles can be attributed to the tendency of the AgNPAs to conglomerate due to their great surface energy and great surface tension of the ultrafine nanoparticles[25].

Table 1 — Structural parameters of AgNPAs.

Structural parameters of silver nanocrystallite		AgNPAs/mesoPS	AgNPAs/macroPS
		hcl (JCPDS) file No. 03-0921	*hcl* (JCPDS) file No. 03-0921
		(111) silver	(111) silver
2θ (degree)	Experimental	38.4	38.28
	(JCPDS)	38.1	38.1
d-space (nm)	Experimental	0.234	0.235
	(JCPDS)	0.2359	0.2359
a (nm)	Experimental	0.4052	0.407
	(JCPDS)	0.4074	0.4074
β (radians)		0.0085	0.009
D_P (nm)		17.26	16.3
S (m^2/g)		33.14	35.09

3.5 SERS of AgNPAs/mesoPS and AgNPAs/macroPS

Figure 8 shows the Raman spectra of R6G adsorbed on (a) fresh mesoPS substrate and (b) fresh macroPS substrate at 10^{-4} M concentration of dye solution. The substrates of fresh PS exhibit a very low Raman signal.

Figure 9 manifests the SERS spectra of R6G dye excited at 532 nm at R6G dye solution concentration of 10^{-6} M adsorbed on AgNPAs/mesoPS and AgNPAs/macroPS substrates. The peaks appearing at 637, 708, 945, 1215, 1294, 1371, 1530 and 1660 cm^{-1} are the characteristic Raman lines of R6G molecules. The SERS spectra of R6G on AgNPAs/mesoPS and AgNPAs/macroPS substrates can be compared with other works[3, 26].

The *EF* is calculated using the following equation[27]:

$$EF = \frac{I_{SERS}/C_{SERS}}{I_{RS}/C_{RS}} \quad \ldots (8)$$

where, I_{SERS} is the SERS signal with a certain concentration of $C_{SERS,}$ and I_{RS} is the Raman signal under non–SERS conditions with a concentration of $C_{RS.}$ In this study, I_{RS} and I_{SERS} were determined using the highest peak of ~1660 cm^{-1} as a reference peak on AgNPAs/mesoPS and AgNPAs/macroPS. It is found that the value of the *EF* achieved by using AgNPAs/macroPS substrate is two orders of magnitude higher than that of AgNPAs/mesoPS substrate of about (1.8×10^6) and (3.2×10^4), respectively.

This can be attributed to the difference between the morphology of the AgNPAs deposited on macroPS and mesoPS, since it is found that AgNPAs deposited on macroPS are more condensed and the dispersion in size of particles deposited on macroPS is less than that of particles deposited on mesoPS. Therefore, the interspacing boosted much stronger SERS "hotspots".

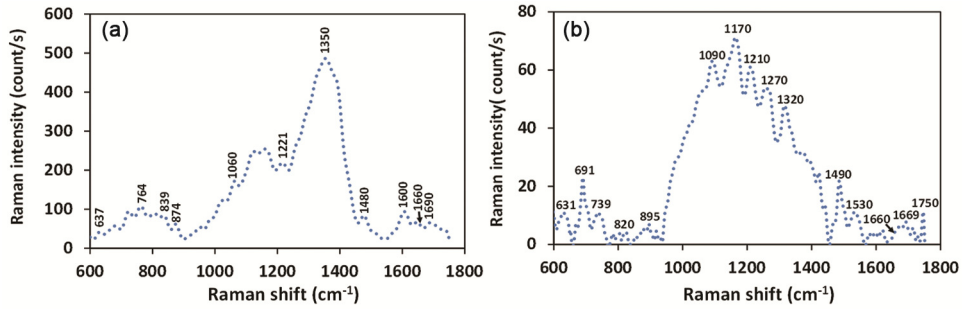

Fig. 8 — Raman spectra of R6G dye at concentration of 10^{-4} M adsorbed on (a) mesoPS and (b) macroPS substrates.

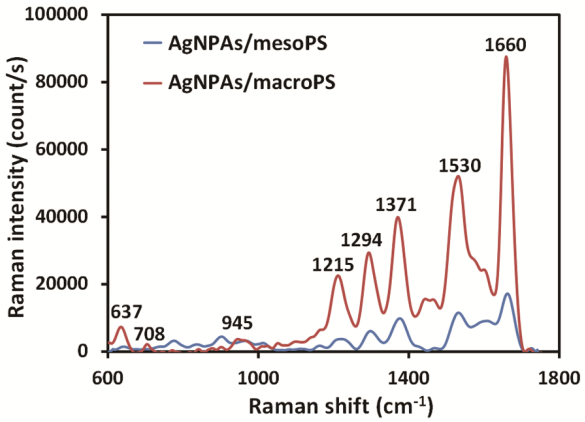

Fig. 9 — SERS spectra of R6G dye adsorbed on AgNPAs/mesoPS and on AgNPAs/macroPS at fixed dye solution concentration of 10^{-6} M and fixed immersion time of 16 min.

4 Conclusions

In summary, AgNPAs/mesoPS and AgNPAs/macroPS were prepared by immersion process of PS samples in $AgNO_3$ solution. The sizes and morphology of AgNPAs depend on the underlying substrate morphology. AgNPAs were deposited on the two kinds of substrates, namely mesoPS and macroPS, in the case of using mesoPS substrate, the AgNPAs couldn't enter inside the pores, therefore they aggregated on the surface of the mesoPS, while in the case of using macroPS substrate, the AgNPAs decorated the inner of the pores, the pores are completely filled with them, and the separated Ag nanoaggregates are formed on the macroPS surface. Thus, AgNPAs can be prepared with specific sizes by controlling the surface morphology of PS substrate. Highest Raman intensity is obtained for AgNPAs/macroPS substrate comparing with AgNPAs/mesoPS by two orders of magnitude. The SERS efficiency of substrate is strictly related to the morphology of PS layer at fixed immersion plating parameters.

Acknowledgment

Authors would like to express their gratitude to the Department of Applied Sciences/University of Technology for assistance with samples preparation.

References

1 Dian J, Macek A, Nižňanský D, Němec I, VrkoslavV, Chvojka T & Jelınek I , *Appl Surf Sci*, 238 (2004) 169.
2 Giorgis F, Descrovi E, Chiodoni A, Froner E, Scarpa M, Venturello A & Geobaldo F, *Appl Surf Sci*, 254 (2008) 7494.
3 Chursanova M, Germash L, Yukhymchuk V, Dzhagan V, Khodasevich I & Cojoc D, *Appl Surf Sci*, 256 (2010) 3369.
4 Zhang T, Song Y J, Zhang X Y & Wu J Y, *Sensors*, 14 (2014) 5860.
5 Nativ-Roth E, Rechav K & Porat Z E, *Thin Solid Films*, 603 (2016) 88.
6 Pavesi L & Turan R, *Silicon nanocrystals: Fundamentals, synthesis and applications*, (John Wiley & Sons), 2010.
7 Kaneko K, *J Memb Sci*, 96 (1994) 59.
8 Jakubowicz J, *Superlatt Microstruct*, 41 (2007) 205.
9 Losic D & Santos A, *Electrochemically engineered nanoporous materials: Methods, properties and applications*, (Springer), 2015.
10 Ouyang H, Christophersen M & Fauchet P M, *Physica Status Solidi A*, 202 (2005) 1396.
11 Le R E, Blackie E, Meyer M & Etchegoin P G, *J Phys Chem C*, 111 (2007) 13794.
12 Tao A R, Habas S & Yang P, *Small*, 4 (2008) 310.
13 Feng F, Zhi G, Jia H S, Cheng L, Tian Y T & Li X J, *Nanotechnology*, 20 (2009) 295501.
14 Xie W & Schlücker S, *Rep Prog Phys*, 77 (2014) 116502.
15 Bisi O, Ossicini S & Pavesi L, *Surf Sci Rep*, 38 (2000) 1.
16 Manilov A & Skryshevsky V, *Mater Sci Eng B*, 178 (2013) 942.
17 Wang C, Liu B & Dou X, *Sens Actuators B Chem*, 231 (2016) 357.
18 Skoog D A, West D M, Holler F J & Crouch S R, *Fundamentals of analytical chemistry*, (Nelson Education), 2013.
19 Hwang J, Hwang S, Chou C & Chen Y, *Thin Solid Films*, 519 (2011) 2313.
20 Lin J C, Chen W L & Tsai W C, *Optics Express*,14 (2006) 9764.
21 Panarin A Y, Terekhov S, Kholostov K & Bondarenko V, *Appl Surf Sci*, 256 (2010) 6969.
22 Wang Y Q, Ma S, Yang Q Q & Li X J, *Appl Surf Sci*, 258 (2012) 5881.

23 Kim H & Cho N, *Nanoscale Res Lett*, 7 (2012) 1.
24 Bykkam S, Ahmadipour M, Narisngam S, Kalagadda V R & Chidurala S C, *Adv Nanopart*, 4 (2015) 1.
25 Theivasanthi T & Alagar M , *arXiv preprint arXiv:*11110260 (2011).
26 Virga A, Rivolo P, Frascella F, Angelini A, Descrovi E, Geobaldo F & Giorgis F, *J Phys Chem C*, 117 (2013) 20139.
27 Botta R, Upender G, Sathyavathi R, Rao D N & Bansal C, *Mater Chem Phys*, 137 (2013) 699.